ANNUAL TRANSACTIONS OF THE NORDIC RHEOLOGY SOCIETY, VOL. 21 (2013) 35

Thermal convection in a nonlinear non-Newtonian magnetic fluid

David Laroze[1,2] and Harald Pleiner[1]

[1]Max Planck Institute for Polymer Research, D 55021 Mainz, Germany
[2]Instituto de Alta Investigación, Universidad de Tarapacá, Casilla 7D, Arica, Chile

ABSTRACT

We report theoretical and numerical results on the convection of a magnetic fluid in a viscoelastic carrier liquid. The non-Newtonian material properties are taken care of by a general hydrodynamic nonlinear viscoelastic model that contains, but is more general than the standard Oldroyd and Giesekus phenomenological rheological equation for the stress tensor. We explore the nonlinear behavior beyond the linear threshold using a truncated Galerkin expansion. As a result, a set of ten equations is obtained describing the time evolution of the mode amplitudes, which can be viewed as a generalized Lorenz system. We find numerically the system's stationary, periodic, multiple-periodic, quasi-periodic, weakly chaotic, and chaotic regimes by investigating power spectra, bifurcation diagrams, and phase portrays. The various types of dynamical behavior are discussed as a function of the Rayleigh number, the magnetic field strength, and the linear and nonlinear viscoelastic material parameters, like relaxation times and elastic moduli.

INTRODUCTION

Ferrofluids are magnetic fluids formed by a stable colloidal suspension of magnetic nano particles dispersed in a carrier liquid. Without an applied external magnetic field the orientations of the magnetic moments of the particles are random resulting in a vanishing macroscopic magnetization (magnetic disorder). An external magnetic field, however, easily orients the particle magnetic moments and a large (induced) magnetization is obtained. In the last decades much efforts have been dedicated to the study of the convective mechanisms in ferrofluids. In particular, heat transfer through magnetic fluids has been one of the leading areas of scientific study due to its technological applications [1]. The ferrofluid convection has applications in high-power capacity transformer systems, where the ferrofluid is used as a material in the core as well as a coolant in the transformer. An important application of ferrofluids lies in the biomedicine area where the carrier liquid is blood [2–6] which is known to have also special rheological proprieties [7–9]. In addition, when a magnetic field is applied, a ferrofluid can acquire additional rheological properties such as magneto-viscosity, adhesion, and other non-Newtonian behavior [10–19]. Hence, a detailed study of viscoelastic magnetic fluids is quite important and in order.

Several experiments of convection in ferrofluids have been reported [20–31], despite the fact that simple optical observations of flow patterns are hampered by the black appearance of the material. Thermal anemometry [21], micro thermistors [26], and small angle neutron scattering [22] can be used, instead.

Viscoelastic properties of fluids can be described by a constitutive equation, which relates the stress and strain rate tensors. The simplest constitutive equation capable of describing realistically the viscoelastic properties is given by the so-called Oldroyd model [32]. It has been found that, besides the usual stationary convection, also

oscillatory states can be obtained at onset. Which type of convection - stationary or oscillatory - appears first, will depend on the values of the rheological parameters. Experimental measurements of oscillatory convection in viscoelastic mixtures were reported by Kolodner [33] in a DNA suspension; and theoretical studies of the convection thresholds for binary Oldroyd mixtures in different types of fluids, can be found in Refs. [34–38]. Recently, studies on stationary and oscillatory convection in Oldroyd magnetic fluids have been done [39–42]. By a somewhat different approach, a generalized prototype model for non-Newtonian fluids was presented by Pleiner et.al. (PLB) in Ref. [43] to describe the rheology of viscoelastic fluids in terms of the strain tensor. The authors obtained a valid hydrodynamic description of viscoelasticity for arbitrarily large deformations, rotations and flow. Taking the solid limit correctly the structure of the equations is determined completely. In addition, typical viscoelastic models, such as Maxwell, Oldroyd, Giesekus, etc. are contained in the PLB model in certain limits. We use this prototype model and focus on the nonlinear system in the case of two dimensional solutions (roll patterns). We show that the system can exhibit stationary, oscillatory and chaotic regimes depending on the control parameters.

BASIC EQUATIONS

We consider an (infinte) horizontal layer of thickness d of an incompressible magnetic ferrofluid with a viscoelastic carrier liquid in a vertical gravitational field $\mathbf{g} = g\hat{\mathbf{z}}$ and subject to a positive temperature difference β across the layer (heating from below). An external magnetic field $\mathbf{H}_0$ is assumed along the vertical direction. Within the Boussinesq approximation, the dimensionless equations for the perturbations from the convection-free, heat conducting state can be written as

$$\boldsymbol{\nabla}\cdot\mathbf{v} = \mathbf{0} \tag{1}$$

$$P^{-1}d_t\mathbf{v} = -\boldsymbol{\nabla}p - \boldsymbol{\nabla}\cdot\boldsymbol{\sigma} + Ra\,\boldsymbol{\Sigma}(\theta,\phi) \tag{2}$$

$$d_t\theta = v_z + \nabla^2\theta \tag{3}$$

$$(\partial_{zz} + M_3[\partial_{xx} + \partial_{yy}])\phi - \partial_z\theta = 0 \tag{4}$$

$$\nabla^2\phi_{ext} = 0 \tag{5}$$

with the abbreviation $\boldsymbol{\Sigma} = M_1(\boldsymbol{\nabla}\theta)(\partial_z\phi) + \hat{\mathbf{z}}(\theta + M_1[\theta - \partial_z\phi])$. Here $\{\mathbf{v},\theta,\phi\}$ are the dimensionless velocity, temperature, and magnetic potential perturbation, respectively. The perturbation equation for U_{ij} reads

$$\begin{aligned} d_tU_{ij} - D_{ij} + U_{ki}\nabla_j v_k + U_{kj}\nabla_i v_k = \\ -\frac{1}{\Gamma_1}U_{ij} - \frac{1}{\Gamma_2}U_{ik}U_{jk}. \end{aligned} \tag{6}$$

This implies for the stress tensor in Eq. (2)

$$\begin{aligned} \sigma_{ij} = &- E_1U_{ij} + E_2U_{ik}U_{jk} - 2D_{ij} \\ &- Z(U_{ik}D_{jk} + U_{jk}D_{ik}) \end{aligned} \tag{7}$$

In Eqs. (1)–(7), the following dimensionless numbers have been introduced, the Rayleigh number, $Ra \sim \beta$, accounting for buoyancy effects due to the heating; the Prandtl number, P, relating viscous and thermal diffusion time scales; the strength of the magnetic force relative to buoyancy, measured by the parameter $M_1 \sim H_0^2$; the nonlinearity of the magnetization, $M_3 - 1 \sim H_0^2$, a measure for the deviation of the magnetization curve from the linear behavior; the linear and nonlinear relaxation times $\Gamma_{1,2}$ and elastic moduli $E_{1,2}$, and the nonlinear viscosity Z, which are all positive.

On the linear level ($\Gamma_2 = E_2 = Z = 0$) it is easy to recover the standard (linear) Oldroyd model

$$(1 + \Gamma\partial_t)\,\sigma_{ij} = (1 + \Lambda\partial_t)D_{ij} \tag{8}$$

containing the Deborah number Γ and the retardation number, Λ. Both descriptions are equivalent with $\Gamma = \Gamma_1$ and $\Lambda = (1 + E_1\Gamma_1)^{-1}$, revealing however that Λ is restricted to $0 < \Lambda < 1$. The kinematic viscosity ν_1, used to scale the time in the viscoelastic description, is related to the

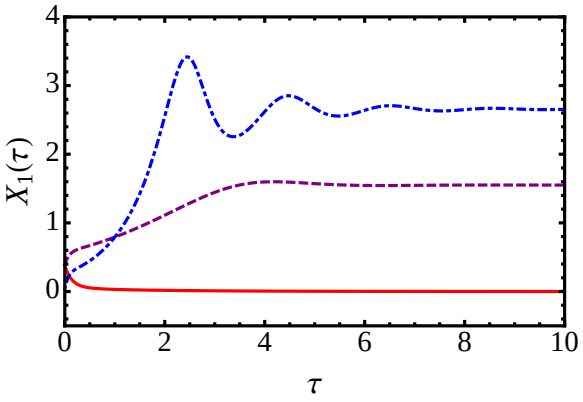

Figure 1: (Color Online) The time dependence of the stream function amplitude in the stationary regime for three different values of r - the continuous, dashed, and dash-dotted curves are for $r = (0.5, 1.5, 2.5)$, respectively, for $M_1 = 10$ and $M_3 = 1.1$. The other fixed parameters are $k = \pi/\sqrt{2}$, $P = 10$, $E_1 = 10$, $E_2 = 1$, $Z = 0.5$, $\Gamma_1 = 0.1$ and $\Gamma_2 = 0.1$.

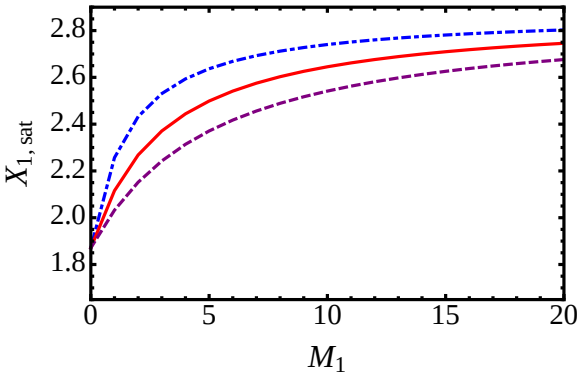

Figure 2: (Color Online) The saturation value $X_{1,sat} = X_1(\tau \to \infty)|$ as a function of M_1 for three different values of M_3 - the dashed, continuous, and dash-dotted curve are for $M_3 = (0.5, 1.0, 3.5)$, respectively, at $r = 2.5$. Other fixed parameters as in Fig. 1

asymptotic viscosity ν_∞ (used in the Oldroyd case) by $\nu_\infty = \nu_1/\Lambda$.

TWO DIMENSIONAL SYSTEM

In this section we solve numerically the system of equations using a truncated Galerkin method. For the sake of simplicity, the analysis is limited to two-dimensional flows, $\mathbf{v} = \{-\partial_z\psi, 0, \partial_x\psi\}$ introducing the stream function ψ. In particular, we assume periodicity with wave number k in the lateral direction, x, describing 2-dimensional convection rolls parallel to the y-axis. By the definition and symmetry of U_{ij}, we only have three components in the 2-dimensional case.

We impose idealized thermal and magnetic boundary conditions [42] and assume rigid boundary conditions for the stream function and the strain tensor components at $z = \{0, 1\}$. For the numerical solution we will restrict ourselves to the fundamental mode in the lateral direction, neglecting higher harmonics, while in the z-direction across the layer a multimode description will be used that fulfills the boundary conditions, automatically [44, 45].

Substituting the trial functions into the dynamic equations and multiplying these equations by the orthogonal eigenfunctions and integrating over a convection cell, yields a set of ten ordinary differential equations for the time evolution of the amplitudes. They are solved via a standard fourth order Runge-Kutta integration scheme with a fixed time step $dt = 0.01$ guaranteeing a precision of 10^{-8} for the amplitudes. For each set of parameters we evolve the numerical solutions at 10^6 time steps in order to avoid observing purely transient phenomena. This system is a generalization of the Lorenz system, hence we expect that the system can exhibit complex behaviors.

NUMERICAL RESULTS

Fig. 1 shows the normalized stream function amplitude, X_1, as a function of time τ for three different values of Ra. After a transient, X_1 tends to a stationary value, which is zero for $r < 1$ and, for $r > 1$, finite and increasing with increasing r. Here, r is the Ra number normalized by the stationary threshold value Ra_{sc} [42]. In Fig. 2 the magnetic field dependence of the saturation amplitude value $X_{1,sat} = X_1(t \to \infty)$ at $r = 2.5$ is shown for three different values of M_3. The amplitude increases with a power law $[X_{1,sat}(M) - X_{1,sat}(0)] \sim {M_1}^{1/\xi}$, where ξ

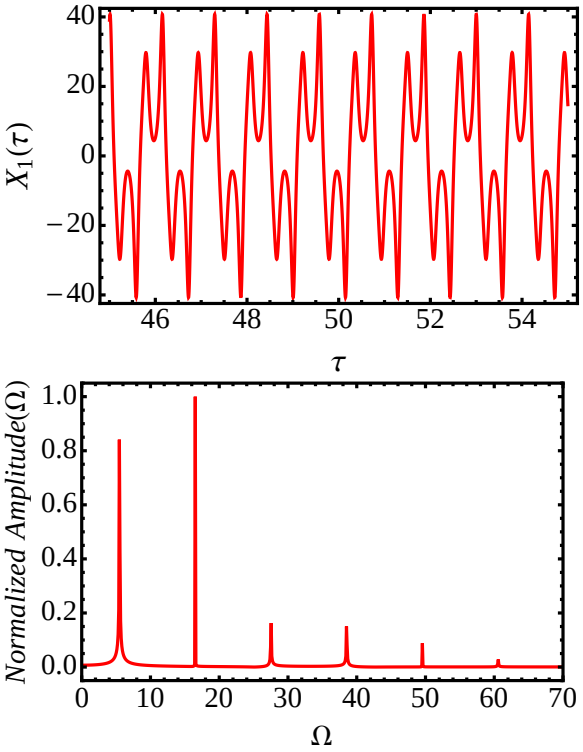

Figure 3: Amplitudes in a periodic regime at $r = 95$, $M_1 = 10$, $M_3 = 1.1$. At the top the time dependence of X_1 is shown and at the bottom the corresponding normalized Fourier power spectrum is plotted. The other fixed parameters are as in Fig. 1.

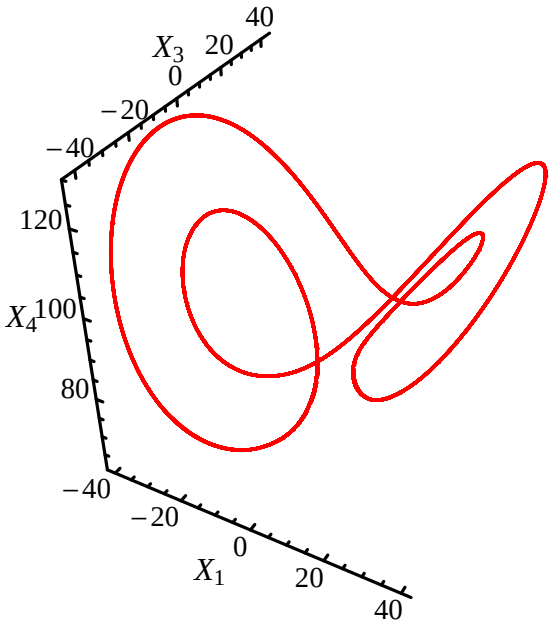

Figure 4: 3D phase portrait of $\{X_1, X_3, X_4\}$ for the periodic regime shown in Fig. 3.

depends on r and the rest of the material parameters. Obviously, a magnetic field has a destabilizing effect increasing the saturation amplitude.

Figures 3 and 4 show the system in a periodic state, which is obtained for higher r. In Fig. 3 the time dependence of the normalized stream function, X_1, is shown in the top frame, while the bottom frame shows the corresponding normalized Fourier power spectrum. There are odd higher harmonic peaks in the spectrum, $\Omega_n = \Omega_0(2n + 1)$, such that Ω_1 is highest and those for $n \geq 2$ are unimportant. A 3D phase portrait of $\{X_1, X_3, X_4\}$ for this state is shown in Fig. 4. It describes a stable non-symmetric $X_1^2 X_3^2$ orbit in the Sparrow notation [46].

Figures 5 and 6 show the system in a different periodic state, which is obtained for rather low r values, but for higher elastic moduli, E_1 and E_2. Again, the time dependence of the normalized stream function, X_1, is shown in the top frame and its corresponding normalized Fourier power spectrum in the bottom frame. Here, the fundamental peak is the most important one, while the odd higher harmonic peaks are pairwise reduced in height. The appropriate 3D phase portrait of $\{X_1, X_3, X_4\}$ in Fig. 6 shows a non-symmetric homoclinic orbit. Clearly, this periodic state at high elastic moduli is different from the one obtained at a high r number.

Figures 7 and 8 show the system in a chaotic regime at a rather low r value. The aperiodic time behavior is manifest in the upper part of Fig. 7, while the lower part reveals the continuos nature of the corresponding Fourier power spectrum indicating the chaotic nature of this state. Figure 8 shows the appropriate 3D phase portrait having the form of a strange attractor similar to the Lorenz attractor. It should be noted that this chaotic state comes at a much lower r value than the periodic one of Figs. 3 and 4 (with all other parameters

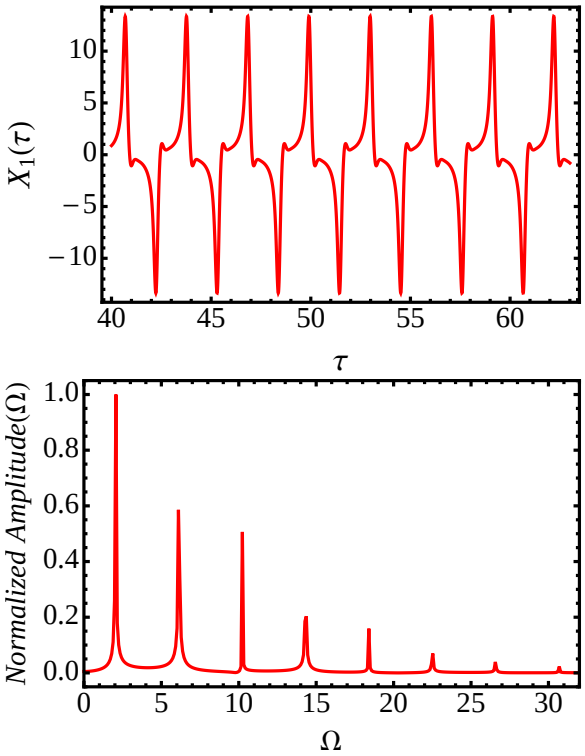

Figure 5: Amplitudes in a periodic regime obtained at higher elastic moduli, $E_1 = 500$, $E_2 = 100$, but lower $r = 13$. At the top the time dependence of X_1 is shown and at the bottom the corresponding Fourier power spectrum is plotted. The other fixed parameters are as in Fig. 1 except for $Z = 3$.

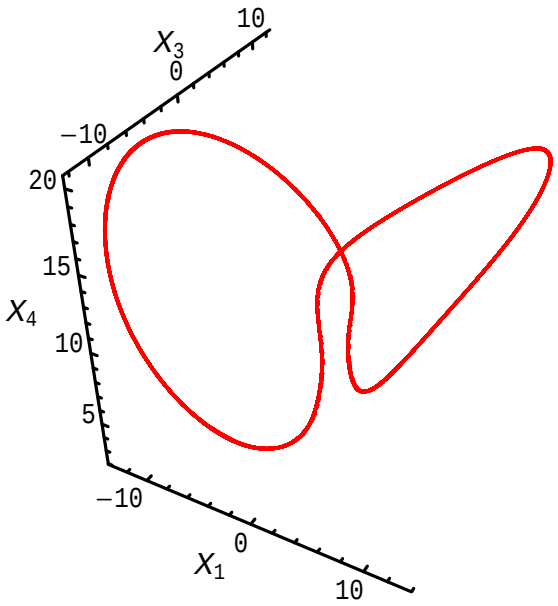

Figure 6: 3D phase portrait of $\{X_1, X_3, X_4\}$ for the periodic regime shown in Fig. 5.

identical). This indicates a rather complicated bifurcation behavior as a function of r with alternating chaotic and periodic states. A comprehensive discussion of the complex bifurcation diagram will be given elsewhere.

Here, we will show the bifurcation diagrams as a function of the linear elastic modulus E_1 and of the nonlinear viscosity Z in Figs. 9 and 10, respectively. These diagrams are obtained by calculating the time series of the amplitudes for many different, random initial conditions. Taking the local maximum values within a certain time slot of, e.g., $|X_1(\tau)|$ reveals the difference between a regular (stationary or oscillatory) and a chaotic behavior. in the former case only one or a few maximum values are found, while in the latter one a continuous-like assembly of such maximum values is present. The bifurcation diagram as a function of the elastic modulus E_1 shows chaos to only exist for intermediate values of E_1, while for small and large ones regular (stationary and oscillatory) behavior is found. Increasing E_1 further the convection amplitude decreases due to the enhanced stiffness of the fluid. In addition, a large nonlinear viscosity (large Z) suppresses chaos and reduces the convection amplitude in an almost discontinuous manner as is shown in Fig. 10.

SUMMARY

In the present work, Rayleigh-Benard convection in a magnetic viscoelastic liquid is studied. For the viscoelastic properties the PLB model [43] is used. Similar to the Lorenz approach [44], a set of ten coupled linear ordinary differential equations is obtained. In the case of the stationary bifurcation we observe that the absolute value of the stream function amplitude (related to the velocity) increases with the external field and is independent of the viscoelastic properties. Due to the viscoelastic properties the system also has an oscillatory bifurcation. We discuss two dif-

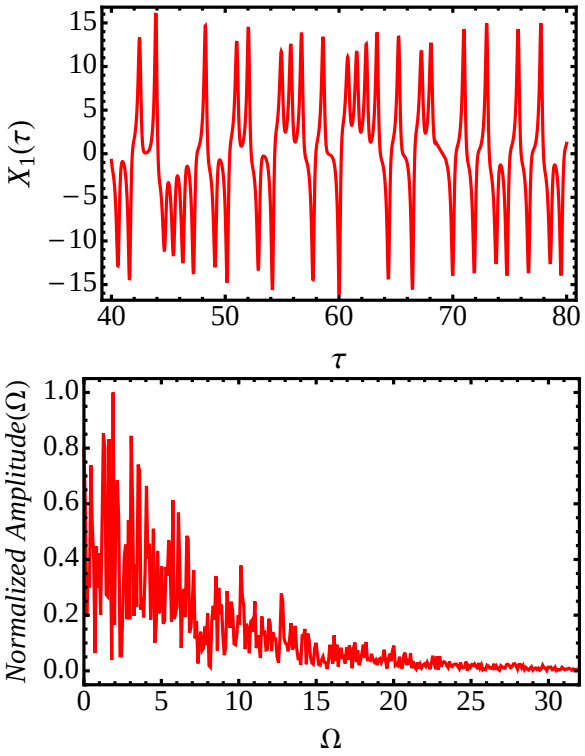

Figure 7: Amplitudes in a chaotic regime at a rather low $r = 13$. At the top the time dependence of X_1 is shown and at the bottom the corresponding normalized Fourier power spectrum is plotted. The fixed parameters are as in Fig. 1.

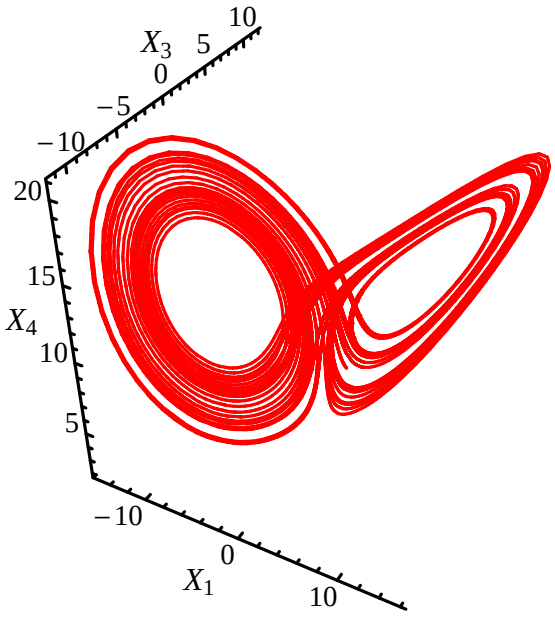

Figure 8: The appropriate 3D phase portrait of $\{X_1, X_3, X_4\}$ in a chaotic regime of Fig. 7.

ferent periodic states, one at high Rayleigh number and low elastic moduli and vice versa. They are rather different, in particular in their nonlinear, higher harmonic behavior. In addition, chaotic behavior is found. It can already occur at rather small Rayleigh numbers, but period states at higher Rayleigh numbers occur in-between chaotic ones. The existence range for chaos strongly depends on the material properties, in particular on the viscoelastic and magnetic ones. The chaotic regime has been characterized by using bifurcation diagrams and Fourier power spectrum calculations, as well as phase portraits.

ACKNOWLEDGEMENTS

D.L. acknowledges the partial financial support from FONDECYT 1120764, Basal Program Center for Development of Nanoscience and Nanotechnology (CEDENNA), Millennium Scientific Initiative, $P10 - 022 - F$ and UTA-Project 8750-12.

REFERENCES

[1] B.M. Berkovsky, V.F Medvedev and M.S. Krakov, *The Magnetic Fluids, Engineering Application*, (Oxford University Press, Oxford 1973).

[2] M. Mahmoudi, M. Shokrgozar, A. Simchi, M. Imani, A. Milani, P. Stroeve, H. Vali, U.O. Häfeli, P. Sasanpour, S. Bonakdar, Multiphysics flow modeling and in vitro toxicity of iron oxide nanoparticles coated with poly(vinyl alcohol), J. Phys. Chem. C **113**, 2322-2331 (2009).

[3] E. H. Kim, Y. Ahn and H. S. Lee, Biomedical applications of superparamagnetic iron oxide nanoparticles encapsulated within chitosan, J. Alloys and Compounds, **434**, 633-636 (2007).

[4] C. Alexiou, R. Jurgons, R.J. Schmid, C. Bergemann, J. Henke, W. Erhardt, E. Huenges, F. Parak, Magnetic drug targeting - Biodistribution of the magnetic carrier and the chemotherapeutic agent mitoxantrone after locoregional cancer treatment, J. Drug Targeting **11**, 139-149 (2003).

[5] C. Alexiou, A. Schmidt, P. Hulin, R.J. Klein, Ch. Bergemann, W. Arnold, W., Magnetic

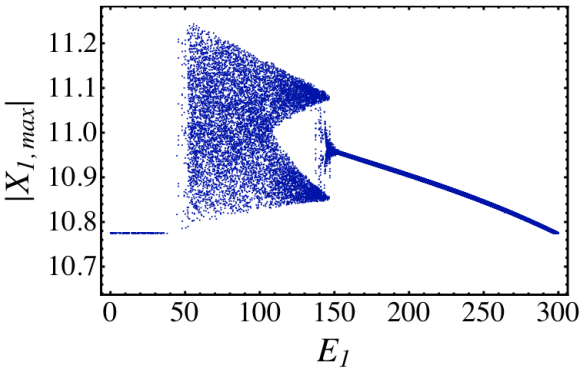

Figure 9: The bifurcation diagram of X_1 as a function of E_1 at $r = 8$ and $E_2 = 1.5$. All other parameters as in Fig. 1.

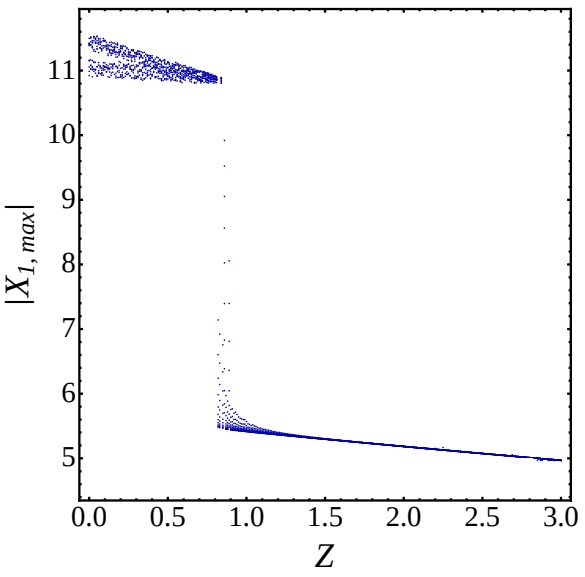

Figure 10: The bifurcation diagram of X_1 as a function of Z at $r = 8$ and $E_1 = 100$. All other parameters as in Fig. 1.

drug targeting: Biodistribution and dependency on magnetic field strength, J. Magn. Magn. Mater. **252**, 363-366 (2002).

[6] C. Alexiou, W. Arnold, R.J. Klein, F. Parak, P. Hulin, C. Bergemann, W. Erhardt, S. Wagenpfeil, A.S. L§bbe, Locoregional cancer treatment with magnetic drug targeting, Cancer Research **60**, 6641-6648 (2000).

[7] A.S. Popel, P.C. Johnson, Microcirculation and hemorheology, Ann. Rev. Fluid Mech. **37**, 43-69 (2005).

[8] O.K. Baskurt, H.J. Meiselman, Blood Rheology and Hemodynamics, Sem. Throm. Hem. **29**, 435-450 (2003).

[9] J.J. Bishop, Rheological effects of red blood cell aggregation in the venous network: A review of recent studies, Biorheology **38**, 263-274 (2001).

[10] H. Shahnazian et al., Rheology of a ferrofluid based on nanodisc cobalt particles, J. Phys. D: Appl. Phys. **42**, 205004 (2009).

[11] D.Yu Borin, S. Odenbach, Magnetic measurements on frozen ferrofluids as a method for estimating the magnetoviscous effect, J. Phys.: Condens. Matter **21**, 246002 (2009).

[12] S.A. Lira, J.A. Miranda, Field-controlled adhesion in confined magnetorheological fluids, Phys. Rev. E **80**, 046313 (2009)

[13] S.A. Lira, J.A. Miranda, Adhesion properties of chain-forming ferrofluids, Phys. Rev. E **79**, 046303 (2009)

[14] O. Müller, D. Hahn and M. Liu, Non-Newtonian behaviour in ferrofluids and magnetization relaxation, J. Phys.: Condens. Matter **18**, S2623-S2632 (2006).

[15] P. Ilg, M. Kröger, S. Hess, Magnetoviscosity of semidilute ferrofluids and the role of dipolar interactions: Comparison of molecular simulations and dynamical mean-field theory, Phys. Rev. E **71**, 031205 (2005).

[16] S. Odenbach, Recent progress in magnetic fluid research, J. Phys.: Condens. Matter **16**, R1135-R1150 (2004).

[17] H.W. Müller, M. Liu, Structure of ferrofluid dynamics, Phys. Rev. E **64**, 061405 (2001).

[18] B.J. de Gans, C. Blom, A.P. Philipse, J. Mellema, Linear viscoelasticity of an inverse ferrofluid, Phys. Rev. E **60**, 4518-4527 (1999).

[19] S. Odenbach, Microgravity research as a tool for the investigation of effects in magnetic fluids, J. Mag. Mag. Mat. **201**, 149-154 (1999).

[20] D. Braithwaite, E. Beaugnon, and R. Tournier, Magnetically controlled convection in a paramagnetic fluid, Nature **354**, 134-136 (1991).

[21] S. Odenbach, Convection driven by forced diffusion in magnetic fluids, Phys. Fluids **6**, 2535-2539 (1994).

[22] S. Odenbach, D. Schwahn, and K. Stierstadt, Evidence for diffusion-induced convection in ferrofluids from small-angle neutron scattering, Z. Phys. B **96**, 567-569 (1995).

[23] S. Odenbach, Microgravity experiments on thermomagnetic convection in magnetic fluids, J. Magn. Magn. Mater. **149**, 155-157 (1995).

[24] H. Yamaguchi, I. Kobori, Y. Uehata, and K. Shimada, Natural convection of magnetic fluid in a rectangular box, J. Magn. Magn. Mater. **201**, 264-267 (1999).

[25] S. Odenbach, Magnetic fluids - Suspensions of magnetic dipoles and their magnetic control, J. Phys.: Condens. Matter **15**, S1497-S1508 (2003).

[26] S. Odenbach and Th. Völker, Thermal convection in a ferrofluid supported by thermodiffusion, J. Magn. Magn. Mater. **289**,122-125 (2005).

[27] H. Engler and S. Odenbach, Parametric modulation of thermomagnetic convection in magnetic fluids, J. Phys.: Condens. Matter **20**, 204135 (2008).

[28] T. Bednarz, C. Lei, and J.C. Patterson, Suppressing Rayleigh-Benard convection in a cube using a strong magnetic field - Experimental heat transfer rate measurements and flow visualization, Int. Comm. Heat Mass Trans. **36**, 97-102 (2009).

[29] T. Bednarz, J.C. Patterson, C. Lei, and H. Ozoe, Enhancing natural convection in a cube using a strong magnetic field - Experimental heat transfer rate measurements and flow visualization, Int. Comm. Heat Mass Trans. **36**, 781-786 (2009).

[30] A. Bozhko and G. Putin, Thermomagnetic convection as a tool for heat and mass transfer control in nanosize materials under microgravity conditions, Microgravity Sci. Technol. **21**, 89-93 (2009).

[31] M. Lajvardi *et al.*, Experimental investigation for enhanced ferrofluid heat transfer under magnetic field effect, J. Magn. Magn. Mater. **322**, 3508-3513 (2010).

[32] D.D. Joseph, *Fluid Dynamics of Viscoelastic Liquids* Springer, New York (1990).

[33] P. Kolodner, Oscillatory convection in viscoelastic DNA suspensions, J. Non-Newtonian Fluid Mech. **75**, 167-192 (1998).

[34] J. Martinez-Mardones, R. Tiemann, D. Walgraef, Thermal convection thresholds in viscoelastic solutions, J. Non-Newtonian Fluid Mech. **93**, 1-15 (2000).

[35] J. Martinez-Mardones, R. Tiemann and D. Walgraef, Amplitude equation for stationary convection in a binary viscoelastic fluid, Physica A **327**, 29-33 (2003)

[36] D. Laroze, J. Martinez-Mardones, and C. Perez-Garcia, Rotating convection in a binary viscoelastic liquid mixture, Int. J. Bif. Chaos **15**, 3329-3336 (2005).

[37] D. Laroze, J. Martinez-Mardones, J. Bragard and C. Perez-Garcia, Realistic rotating convection in a DNA suspension, Physica A **385**, 433-438 (2007).

[38] D. Laroze, J. Martinez-Mardones, J. Bragard, Thermal convection in a rotating binary viscoelastic liquid mixture, Eur. Phys. J. Special Topics **146**, 291-300 (2007).

[39] D. Laroze, J. Martinez-Mardones, Convection in a Viscoelastic Magnetic Fluid, AIP Conf. Proc. **913**, 9-13 (2007).

[40] D. Laroze, J. Martinez-Mardones and L.M. Pérez, Amplitude equation for stationary convection in a viscoelastic magnetic fluid, Int. J. Bif. Chaos **20**, 235-242 (2010).

[41] D. Laroze, J. Martinez-Mardones and L.M. Pérez, R.G. Rojas, Stationary thermal convection in a viscoelastic ferrofluid, J. Mag. Mag. Mat. **322**, 3576-3583 (2010).

[42] L.M. Pérez, J. Bragard, D. Laroze, J. Martinez-Mardones and, H. Pleiner, Thermal convection thresholds in a Oldroyd magnetic fluid, J. Mag. Mag. Mat. **323**, 691-698 (2011).

[43] H. Pleiner, M. Liu, and H.R. Brand, Nonlinear fluid dynamics description of non-Newtonian fluids, Rheol. Acta. **43**, 502-509 (2004).

[44] E.N. Lorenz, Deterministic Nonperiodic Flow, J. Atmos. Sc. **20**, 130-141 (1963).

[45] A. Ryskin and H. Pleiner, The influence of a magnetic field on the Soret-dominated thermal convection in ferrofluids", Phys. Rev. E **69**, 046301 (2004).

[46] C. Sparrow, *The Lorenz Equations: Bifurcations, Chaos, and Strange Attractors*, (Springer, Berlin 1982).